A Reflection Near-Field Scanning Optical Microscope Technique for Subwavelength Resolution Imaging of Thin Organic Films

Kenneth D. Weston and Steven K. Buratto*

Department of Chemistry, University of California, Santa Barbara, California 93106

Received: November 18, 1996; In Final Form: February 4, 1997[⊗]

A dual mode near-field scanning optical microscopy (NSOM) technique, in which light is both emitted from and collected by a subwavelength aperture, is described and demonstrated. This dual mode configuration is capable of high contrast (via the refractive index) as well as high-resolution optical microscopy in reflection. The contrast in these images is shown to depend strongly on the interference of the light incident to and reflected from the sample surface. We show that with the dual mode configuration the topography induced contrast can be quantitatively separated from the true optical contrast resulting in a mapping of the refractive index of the sample. This separation has proven difficult, if not impossible, for other reflection NSOM geometries. To demonstrate the utility of this technique for thin organic films we present dual mode images of a nine-layer organic/inorganic self-assembled multilayer film on a silicon substrate.

Introduction

Near-field scanning optical microscopy (NSOM), a recently developed technique, has made microscopy and spectroscopy possible with spatial resolution approaching 10 nm.[1,2] This remarkable technique has been used to probe nanoscale optical properties of a variety of samples important in physical chemistry including: conjugated polymer films,[3,4] organized molecular aggregates,[5] molecular crystals,[6] Langmuir−Blodgett films,[7] and semiconductor quantum structures.[8−10] Although all optical contrasts are possible using NSOM,[11] the above systems have relied heavily, if not entirely, on fluorescence contrast. In many important samples, especially organophosphonate self-assembled monolayer and multilayer films, there is not an available chromophore for fluorescence contrast. Optical microscopy of these samples requires contrast via the refractive index which determines the transmissivity and reflectivity of the film. While transmission NSOM has been successfully applied to nonchromophore samples,[12] reflection NSOM has remained largely ignored. The principal reasons for this are the inherently low signal-to-noise ratio of reflection NSOM (compared to transmission NSOM) and the extreme complexity of the resulting image.[13] The complexity results from the convolution of the true optical contrast (refractive index contrast) and the topography induced contrast (z-contrast). In this paper we describe and demonstrate a mode of NSOM which significantly simplifies the image contrast and allows the refractive index contrast to be easily extracted from the image. We establish the utility of this technique in probing the nanoscale refractive index of thin organic films on opaque substrates.

The NSOM technique relies on placing a subwavelength aperture (a tapered optical fiber coated with 100 nm of aluminum[1]) in close proximity (∼15 nm, called the near-field) to the sample being imaged. The light emanating from this aperture rapidly diverges, but remains collimated for approximately one aperture diameter. In this region, the aperture diameter defines the resolution (i.e., the spatial extent of the interaction between the light and the sample surface) and not the wavelength of the light. Like conventional optical microscopy, NSOM can be performed in transmission or reflection. In transmission NSOM, the tip (i.e., aperture) is used to excite the sample and the transmitted or emitted light is collected in the far-field on the opposite side of the sample. For opaque samples, reflection NSOM is employed which differs from transmission NSOM only in that the tip and the detecting (far-field) optics must be on the same side of the sample. This difference is a huge disadvantage in signal-to-noise for the reflection geometry relative to the transmission geometry for two important reasons: (1) the collecting optics must be placed at a sufficient distance from the sample to allow enough space for the tip, and (2) the tip itself obstructs the collecting optic's "view" of the spot irradiated by the tip on the sample.[13] Also, effects of sample topography on the reflection NSOM image have proven to be more prevalent and more complex than in the transmission geometry,[13,14] making image interpretation difficult and the separation of z-contrast from the true optical contrast virtually impossible. In the remainder of this paper we describe how dual mode NSOM is implemented, the effects that make image interpretation easier, and the method for quantitative separation of z-contrast from the refractive index contrast.

Experimental Section

In the experiments described in this paper, three different samples were imaged including: (1) an aluminum grating standard, (2) a 30 nm patterned film of aluminum on glass, and (3) an organic/inorganic self-assembled multilayer (SAM) film on a silicon substrate. The grating standard, which consists of 5 μm × 5 μm × 180 nm deep pits etched into aluminum, was used as a control for z-contrast. The patterned aluminum film was 30 nm thick and consisted of 850 × 850 nm squares arranged in a checkerboard pattern (see Figure 2a). This sample was used as a control sample for true optical (i.e., refractive index) contrast. Z-contrast was negligible in comparison to the optical contrast for this sample due to the large difference in refractive index between the glass and metal. The organic/inorganic SAM film was fabricated by Prof. C. Page and coworkers at the University of Oregon using a metal−bisphosphonate self-assembly technique.[15,16] The film was grown one monolayer at a time by immersing the substrate in a solution of hafnium oxychloride, followed by immersion in a solution of the SAM molecule, aryl-(4-diethylphosphonate)-10-decylphos-

[⊗] Abstract published in *Advance ACS Abstracts,* June 15, 1997.

S1089-5647(96)03856-4 CCC: $14.00

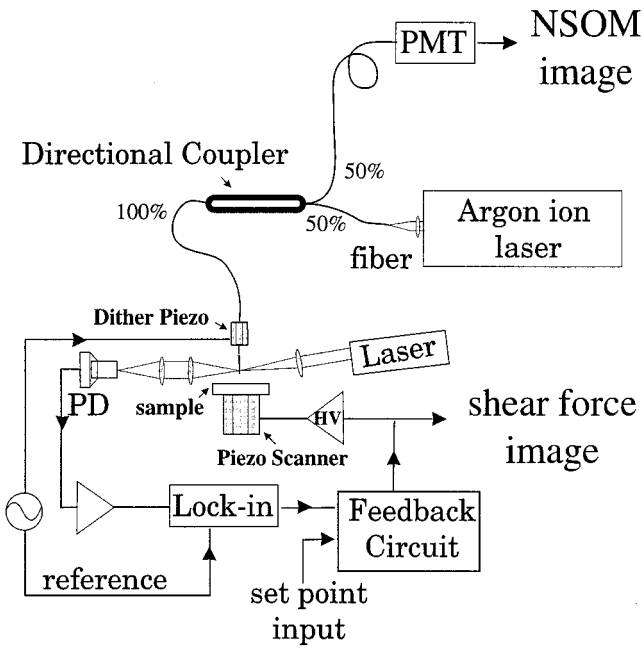

Figure 1. Schematic of the dual mode NSOM setup. The light is coupled into one 50% leg of the directional coupler, travels to the aperture of the NSOM probe, and interacts with a local portion of the sample surface. The reflected light is collected by the same NSOM tip and is detected at the other 50% leg of the directional coupler. The tip−sample gap is maintained with optically detected shear force feedback. The laser, optics, and photodiode (PD) for the shear force feedback are also shown.

phonic acid ether.[16] The molecules were bound to the Hf-primed surface through the phosphonate resulting in oriented assembly, and the reaction was self-limiting to one monolayer. Additional layers were added by first converting the ester group to a phosphonate by acid hydrolysis, priming the new phosphonate surface by immersion in hafnium oxychloride, and then immersing the Hf-primed surface in a solution of the SAM molecule. The sample imaged in this work consisted of a total of nine layers. The thickness of the multilayer film was determined to be 19 nm (equal to nine layers) by ellipsometry.[17] This sample was chosen as a test for the technique because it exhibits a combination of both z-contrast and refractive index contrast in reflection NSOM.

The NSOM apparatus used in the experiments described in this paper has been described in detail in a previous publication.[13] Briefly, the NSOM tip is placed in the near-field and used to illuminate the sample surface. The NSOM tips used in this work were fabricated from single-mode optical fiber (Newport F-SA) and had apertures ranging from 100 to 150 nm in diameter. In illumination mode NSOM, the light reflected from the sample is collected with a microscope objective oriented at a 45° angle to the axis of illumination[13] and routed to a photomultiplier tube (PMT) for detection. Images are produced by raster scanning (0.5 Hz scan rate) the sample while keeping the tip fixed. The piezo tube scanner is computer controlled via commercially available scanning electronics and software (Digital Instruments Nanoscope III). The NSOM tip−sample gap was maintained at about 15 nm using standard, optically detected shear force feedback (see Figure 1).[18,19] The feedback signal provides an independent topography image collected simultaneously with the NSOM image. This image is important for understanding the role of topography in determining NSOM contrast.

In dual mode NSOM, light from an Ar^+ laser was coupled into one of the 50% leads of a fiber optic 1 × 2 bidirectional coupler (Gould Fiber Optics) with the other 50% lead coupled to a PMT and the 100% lead coupled to the NSOM tip as illustrated in Figure 1. As in illumination mode NSOM, the light from the Ar^+ laser was used to illuminate the sample through the tip. Note that we make no attempt to control the polarization of the light in the tip for either imaging mode. After reflection from the sample, the light was collected by the tip, split 1:1 at the bidirectional coupler, and detected at the PMT. It is important to note that in this dual mode geometry light must pass through the aperture twice and is thus strongly attenuated relative to the light initially coupled into the fiber from the Ar^+ laser. Letting I_o denote the intensity of the light launched into the fiber, δ denote the transmission efficiency of the tip, and η denote the collection efficiency of the tip, then the maximum signal (S_{max}), assuming no loss in reflection, is

$$S_{max} = \eta\delta I_o \tag{1}$$

If it is assumed that the transmission efficiency is of the order of 10^{-4} ($\delta = 10^{-4}$),[1] then a large portion of I_o is reflected from the tip taper region and never reaches the sample. If any of this light reaches the PMT then it will add directly to the signal. While this back-reflected light (denoted B) contributes only a dc offset to the signal, it is possible for the shot noise due to this background light ($\sim B^{1/2}$) to dominate the signal. Letting γ be the reflectivity of the NSOM tip (i.e., the proportion of the background light reaching the detector) and assuming no other losses in the fiber, the background signal is

$$B = \gamma I_o \tag{2}$$

We have measured γ to be of the order of $10^{-4}-10^{-5}$. Thus, most of the incident light launched into the fiber never reaches the aperture nor is it reflected back into propagating modes of the fiber such that it is detected at the PMT. It is likely that the largest fraction of the light launched into the fiber is reflected by the tip taper region and is lost in fiber-cladding modes which do not propagate to the detector. We also point out that our measurement of γ differs from a previous measurement by over an order of magnitude.[20] We attribute this discrepancy to the difference in tips (i.e., the shape of the taper region) as we have also observed order of magnitude changes in reflectivity when comparing γ for different tips in our own lab. It is now possible to obtain a rough estimate of the signal-to-background ratio if we approximate the collection efficiency of the tip to be ($\eta = 10^{-3}$),[21]

$$\frac{S_{max}}{B} \approx \frac{10^{-3}10^{-4}I_o}{10^{-5}I_o} = 10^{-2} \tag{3}$$

Experimentally, we have typically observed this ratio to be of the order of 10^{-1} indicating that the surface sensitive signal is much larger than expected by this simple model. The two most probable reasons for this difference are that the tip collection efficiency is much higher than 10^{-3} and that the evanescent modes transmitted by the tip, but not detected in the measurement of δ, contribute to the signal detected in the dual mode geometry. It is also important to note that light reflected back from the coupling junction between the 100% lead of the directional coupler and the tip can further increase the background signal. We have found that a $<2dB$ loss mechanical splice (Thorlabs part # TS-125) is more than adequate, provided that care is taken to ensure a good junction. For most moderate reflectivity (>10%) samples, we have found that it is possible to observe a signal in the dual mode geometry.

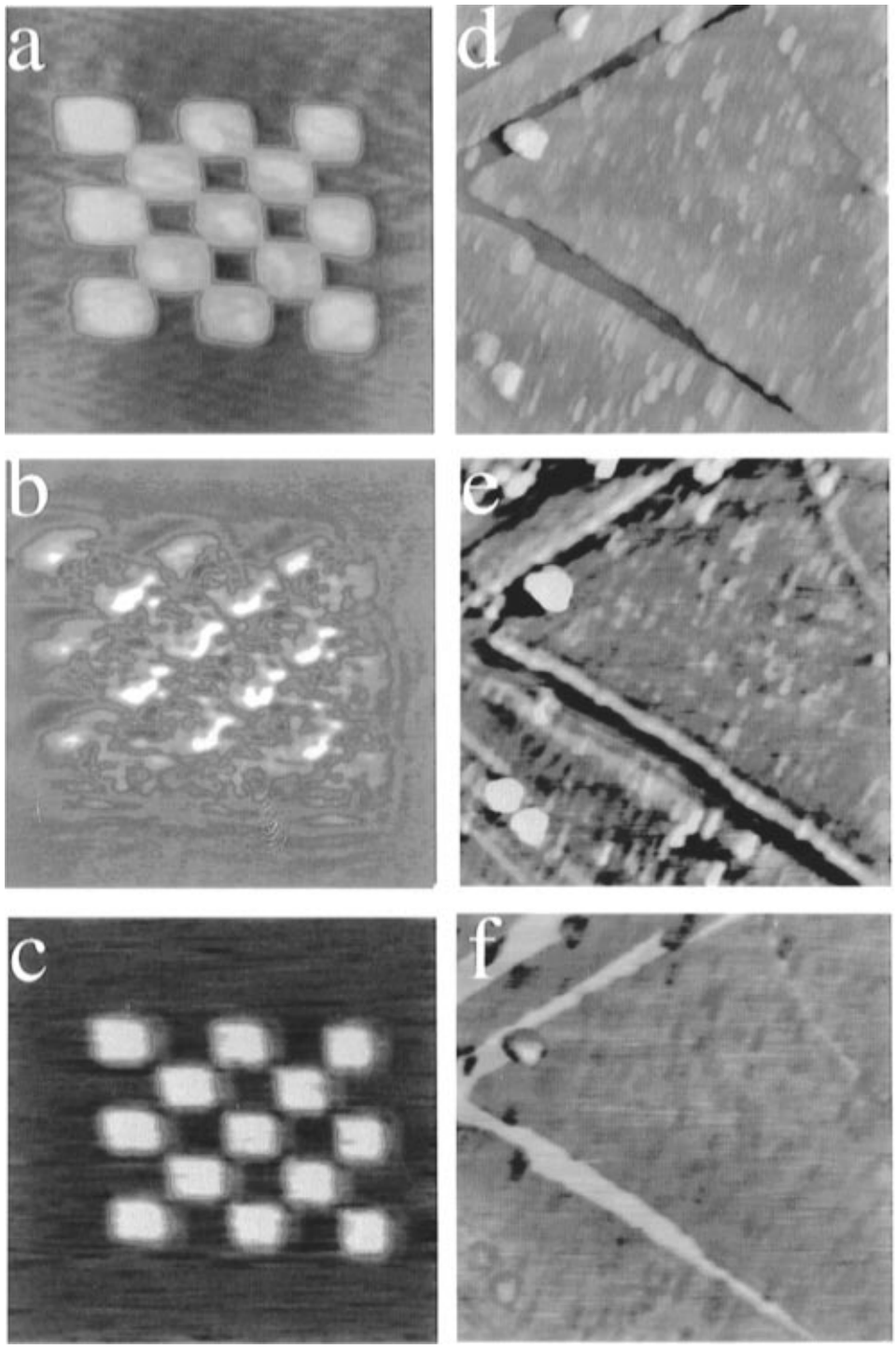

Figure 2. A comparison of dual mode NSOM and illumination mode NSOM images of a patterned Al film on glass (parts a−c) and SAM (parts d−f) samples. The figure includes the topography (a and d), dual mode NSOM images (b and e), and illumination mode NSOM images (c and f) of the two different samples, respectively. *In the color scale of these images, white represents the tallest features in the topography image and the maximum detected signal in the NSOM images.* Note the improvement in clarity of the dual mode images over the illumination mode images. A detailed explanation is given in the text.

For each dual mode image acquired, a plot of the NSOM signal as a function of the tip−sample gap was obtained. This was accomplished by recording the NSOM signal as the sample is moved from the position where the feedback circuit is engaged (∼15 nm from the sample surface but denoted position zero in all such plots) to the fully retracted position. For this reason, the curves will be referred to as NSOM "retract" curves from this point on. Since these curves are important for quantitatively determining z-contrast, care was taken to acquire images immediately before or after acquiring the retract curves so the two could be directly correlated.

Results and Discussion

Images obtained with the dual mode arrangement were found to be less confusing and easier to interpret than those obtained in the conventional illumination mode. To illustrate this point, images of samples 2 and 3 are presented in Figure 2 for both illumination mode NSOM and dual mode NSOM using the same tip. The checkerboard pattern is easily resolved in the dual mode image (Figure 2c), but it is extremely distorted in the illumination mode image (Figure 2b). The distortions and decreased resolution in Figure 2b can be understood as follows.

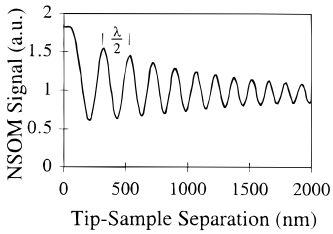

Figure 3. NSOM retract curve. The signal detected oscillates with a spatial period of $\lambda/2$ as a function of the tip−sample gap. Position zero refers to the position where feedback is engaged (∼15 nm from the sample surface). The oscillations result when two counter-propagating waves, the incident and reflected waves, interfere to create a standing wave at the sample surface.

Light exiting the aperture must make several reflections between the sample surface and bottom of the NSOM probe (including the metal coating) to escape to the detector in the far field.[13,14] Topographic features on the sample surface and the roughness of the tip's metal coating cause differences in the path and number of reflections from the illuminated region to the detector. As a result, the amount of light collected and directed to the detector is very sensitive to the topographic features and the image becomes complex and difficult to interpret. Because the light collected interacts with an area of the sample surface larger than the area of the physical aperture, the multiple reflections also decrease the spatial resolution.[14] This effect increases the "effective" aperture size of the reflection NSOM. The image obtained using dual mode NSOM, however, is much less complex and has higher resolution. The reason for the improvement in image contrast and resolution is a decrease in the "effective" aperture of dual mode NSOM over that of illumination mode NSOM. Although the behavior of light in the near-field regime of an NSOM probe is not well understood, it is intuitive to expect that only the light within the spatial dimension of the aperture will be collected efficiently by the aperture. Thus, the "effective" aperture in dual mode NSOM is smaller than in illumination mode NSOM and closer to the actual size of the aperture.

This argument holds true even for samples where the illumination mode NSOM image is not as distorted in the case of sample 2 (Figures 2a−c). Figures 2d−f are the topography, illumination mode NSOM, and dual mode NSOM images, respectively, of the SAM sample (sample 3). The dark intersecting stripes in the topography image indicate a trough approximately 20 nm deep. Since this is the height expected for a nine-layer film, we can assume that the film is either completely absent from this region of the substrate or did not grow beyond one monolayer. While the illumination mode NSOM image of Figure 2e is not as distorted as the illumination mode NSOM image of Figure 2b, clearly topography in the SAM sample has an influence over the illumination mode NSOM contrast. The dual mode NSOM image (Figure 2f) of the SAM is much simpler than the illumination mode NSOM image (Figure 2e), however, it is still unclear from the image of Figure 2f whether the contrast observed is z-contrast, refractive index contrast, or a combination of both. In order to understand the contribution from refractive index contrast and z-contrast in the dual mode NSOM image of this sample, a closer look at the physics governing the dual mode configuration is required and is discussed in the following paragraphs.

An important consequence of the dual mode geometry is the strong influence of interference effects (between the incident and reflected light) on the detected signal. These interference effects are evident in the NSOM retract curve shown in Figure 3. The NSOM signal oscillates with a spatial period of approximately $\lambda/2$ as a function of the tip−sample gap. These oscillations have been observed previously in NSOM experiments with far-field collection[22−24] and dual mode collection using an uncoated fiber tip.[24] The signal level at the initial point of the retract curve, denoted on the plot as position zero, represents the signal level when the tip is engaged in feedback on the sample surface (∼15 nm from the surface). This signal level is extremely important for NSOM imaging since it is the base level signal observed in the image. The contrast in an NSOM image then is determined by the deviation from this base signal. Deviations from this base signal that result from large topography features which alter the tip−sample gap are the cause of z-contrast. The NSOM signal observed near such features can be determined by extrapolating along the NSOM retract curve for a known change in tip−sample gap. Therefore, the retract curve is crucial for proper interpretation of NSOM images.

The oscillations observed in the retract curves of dual mode NSOM are analogous to the fringes observed by Wiener in his famous 1941 experiment.[25] For light propagating normal to a reflective surface the electric field of the incident ($\mathbf{E_i}$) and reflected ($\mathbf{E_r}$) waves are given by

$$\mathbf{E_i} = A e^{[-i(\omega t - kz) + \phi_i]} \qquad \mathbf{E_r} = -RA e^{[-i(\omega t + kz) + \phi_r]} \quad (4)$$

Where the positive z-axis is in the direction of propagation of the reflected wave, A is the amplitude of this incident wave, R is the reflection coefficient of the reflecting material, and ϕ_i and ϕ_r are the phases of the incident and reflected waves, respectively. For an infinitely reflecting surface $R = 1$, $\phi_i = \phi_r = 0$, an intensity I as a function of z is given by

$$I = (\mathbf{E_i} + \mathbf{E_r})^2 = 2A^2\left(1 - \cos\left(2\pi \frac{2z}{\lambda}\right)\right) \quad (5)$$

From eq 5 it is clear that the detected light as a function of z oscillates with a period of $\lambda/2$ as is seen Figure 3.

There are, however, several important differences between the Wiener fringes described by eq 5 and the retract curve in Figure 3. First, there is an envelope associated with the oscillations which is a result of the increased collection efficiency of the tip as the tip approaches the sample surface. Second, the initial point (closest to the sample surface) of the retract curve is not, in general, a node as is predicted from eq 5 and the "phase" of the oscillations is not always zero. In dual mode NSOM, this phase has been observed to have a complicated dependence on the wavelength, the shape of the NSOM tip, and the reflectivity of the sample. For a given sample and wavelength the phase readily changes from tip to tip indicating that it is particularly sensitive to tip aperture size and shape. A more thorough investigation of this phenomena is in progress. In order to predict quantitatively the relationship between the phase detected and the optical properties of the sample surface, a complete description of the mode field pattern emanating from the tip, as well as the modes collected by the NSOM tip, is required. While a number of investigators have calculated the modal fields transmitted by the tip,[26−28] a good model which describes the collection efficiency of the modes has yet to be developed. A more complete understanding of the transmission and collection phenomena in the vicinity of an NSOM probe would allow the refractive index of the sample to be calculated from the retract curve. Furthermore, interpretation of the images produced using the dual mode arrangement will be significantly enhanced by such understanding. In spite of the lack of a quantitative model of the oscillations, however, it is possible to use the retract curve and the topography image

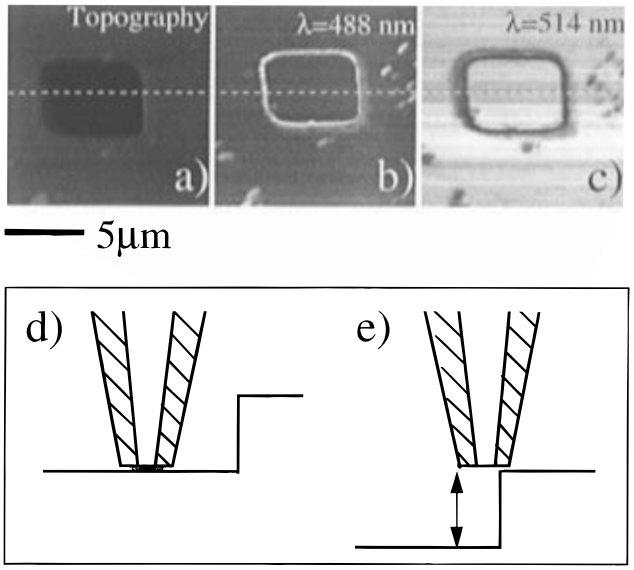

Figure 4. Dual mode NSOM of the grating standard obtained using $\lambda = 488$ nm and $\lambda = 514$ nm, respectively. The sample consists of a smooth metal surface with 5 μm × 5 μm × 180 nm deep wells. The signal changes at the edges of the well due to the NSOM probe straddling the sharp edge and increasing the aperture to sample distance. An illustration of this is shown (d and e). Note that the aperture−sample gap varies at abrupt topographic edges even though a constant tip−sample gap is maintained as shown (e). The contrast reversal between the images of parts d and e is due to the dependence of the phase of the standing wave on wavelength (see text).

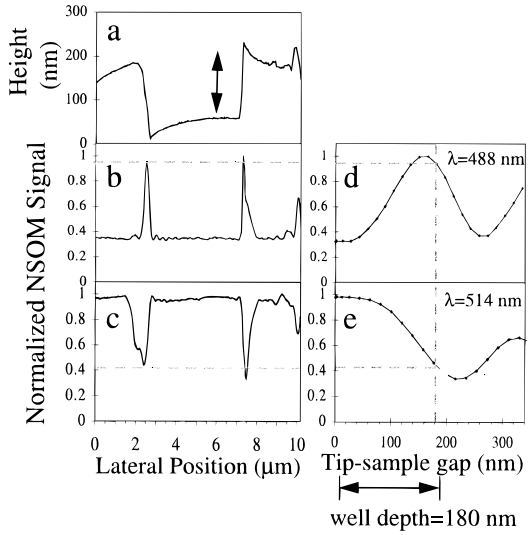

Figure 5. Line traces taken from the images in Figure 4. Traces in parts a, b, and c correspond to the dotted line in Figures 4a−c, respectively. Parts d and e show the oscillations of the NSOM retract curve acquired prior to the images in Figures 4b,c, respectively. The intersection of the vertical dashed line and the NSOM retract curves indicates the NSOM signals when the tip−sample gap is 180 nm (the depth of the well) for $\lambda = 488$ nm and 514 nm, respectively. The horizontal dashed lines relate the signal in the retract curves to the signal in the line traces of parts b and c. The signal level observed when the tip straddles the edges of the well is equal to the signal observed in the retract curves at a tip−sample gap of 180 nm.

to predict the amount of z-contrast in the image as is shown in the next paragraph.

To demonstrate the effects of topography on dual mode NSOM images and to illustrate the importance of the interference effects on image contrast, images of the grating standard using two illumination wavelengths ($\lambda = 488$ and 514 nm) are presented in Figure 4. Figure 4a shows the topography image of one of the pits, Figure 4b is the simultaneously acquired dual mode NSOM image using the $\lambda = 488$ nm line of an Ar^+ laser, and Figure 4c is the dual mode NSOM image using $\lambda = 514$ nm. A striking feature regarding the two NSOM images (Figure 4b,c) is their completely opposite contrast. This contrast reversal is caused by the change in the phase of the retract curve oscillations for the two wavelengths and will be discussed further later in the text. Note that contrast is only observed at the edges of the pits and the detected NSOM signal remains constant as expected since the sample is made of just one material. The deviation in the signal at the edges of the pit is the result of the increased aperture−sample gap which occurs as the tip straddles the sharp edges of the pit. This situation is illustrated in Figure 4 which shows that, even though the tip−sample gap is maintained at a constant value when a sharp edge is encountered, the aperture−sample gap changes (indicated by the arrow in Figure 4e). The increase in aperture−sample distance while tracking a topography feature with a sharp edge has the same effect on the NSOM signal as pulling the sample away from the tip when an NSOM retract curve is acquired. Therefore, it is possible to predict the signal level for a sharp edge of known height by extrapolating along the retract curve. This prediction is verified by the data presented in Figure 5.

Line traces taken from the images of Figures 4a−c are shown in Figures 5a−c, respectively. Figure 5d shows the NSOM retract curve for this sample obtained using $\lambda = 488$ nm just before the image in Figure 4b was acquired. The intersection of the vertical dashed line with the retract curve in Figure 5d shows the NSOM signal level when the tip−sample gap is 180 nm (the depth of the well). This signal level is equal to the signal observed in the NSOM image when the tip straddles the edges of the well as can be seen in the line trace in Figure 5b (follow the horizontal dashed line). The same analysis is also shown to correctly predict the contrast in the image taken using $\lambda = 514$ nm (Figures 5c,e). It is clear that the difference in the phase of the retract curves (Figures 5d,e) obtained for each wavelength is responsible for the reversal of contrast between the two NSOM images. The retract curve for $\lambda = 488$ nm shows the signal increases initially to the first maximum at ∼150 nm, whereas the retract curve for $\lambda = 514$ nm shows the signal decreasing initially to the first minimum at ∼220 nm.

The advantage of using NSOM over other scanned probe microscopies is its sensitivity to the optical properties of a sample. To test dual mode NSOM for the ability to "see" true optical contrast, we imaged the thin (30 nm) patterned film of aluminum on glass. The NSOM image obtained while using $\lambda = 488$ nm is shown in Figure 6a. In Figure 6b, the NSOM retract curves obtained when the tip is placed over the aluminum and those obtained when the tip is placed over the glass far from the pattern are shown. No oscillations in the retract curve are detected when the tip is placed over the glass since the reflectivity at an air−glass interface is only about 4%. A standing wave is created, but it is weak compared to the noise in the experiment. The oscillations are clearly evident in the curve taken when the tip retracts from the aluminum portion of the sample. The arrows indicate points of equal signal level in the image and at position zero of the retract curve. The image of the same sample taken using $\lambda = 514$ nm, as well as the retract curves for this wavelength, is shown in Figures 6c,d. All of the contrast in this image can be accounted for by the signal difference between the glass and the metal (i.e., the initial points of the retract curves for metal and glass), and no significant contributions from z-contrast are observed in the images in Figure 6.

To test the capabilities of dual mode NSOM on a "real" sample, the technique was used to image a nine-layer Hafnium

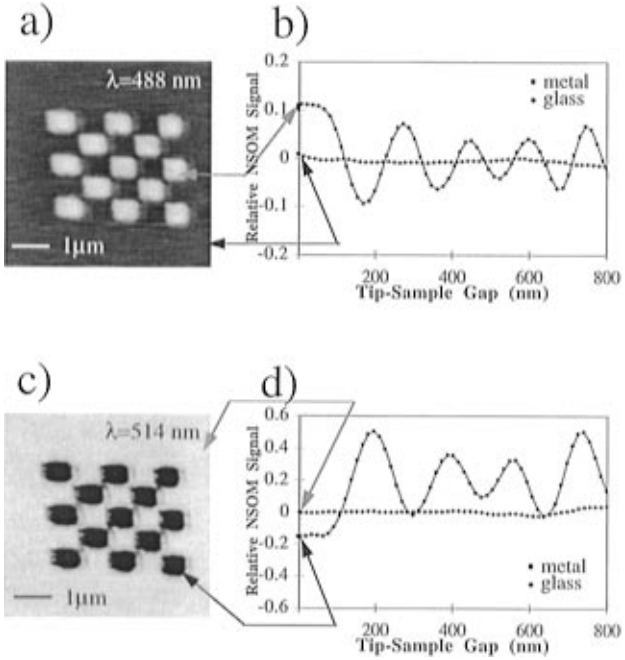

Figure 6. Dual mode NSOM of a thin (25 nm) patterned aluminum film on glass. Images shown in parts a and c were taken using $\lambda = 488$ nm and $\lambda = 514$ nm light, respectively. The NSOM retract curves are shown in parts b and d, respectively, for both the tip positioned over the glass and the tip positioned over the aluminum. The arrows indicate that the signal at position zero in the retract curves corresponds directly to the signal observed in the image. The image contrast is clearly due to the change in reflectivity and not the topography. The contrast reversal results from the phase difference of the oscillations for the two different wavelengths as seen in parts b and d, respectively. Note also that the depth of modulation of the curve is significantly higher when the tip is positioned over the aluminum as expected since the reflectivity of the metal is much higher than that of the glass.

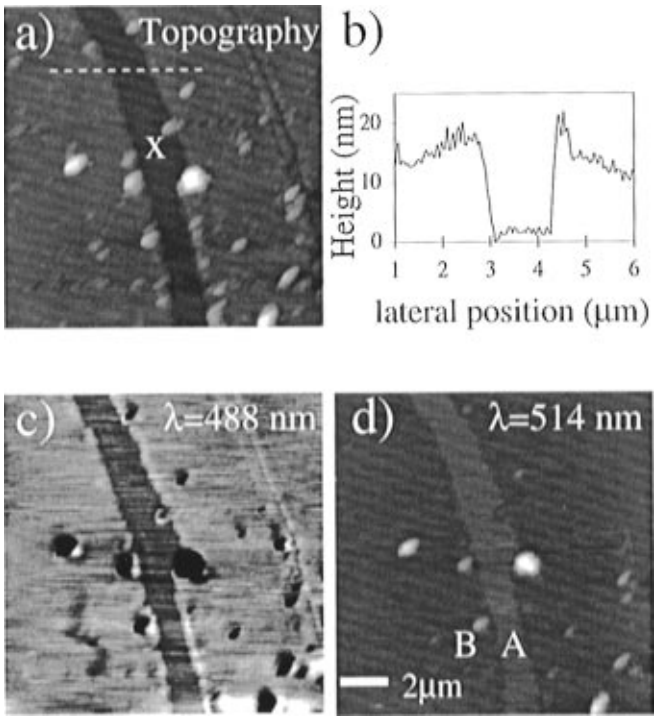

Figure 7. Topography (a), and dual mode NSOM images, (c) and (d), of a nine-layer Hafnium aryl-(4-diethylphosphonate)-10-decylphosphonic acid ether SAM using $\lambda = 514$ nm and $\lambda = 488$ nm light, respectively. A line trace taken from the position indicated by the white dashed line in part a is presented in part b and shows the trough of the image of Figure 7a to be 20 nm deep indicating that the film is either completely absent or did not grow beyond one monolayer. Note also the aggregates observed in part a with dimensions ranging from 50−800 nm in diameter and 10−70 nm in height. The contrast in each NSOM image results from a combination of z-contrast and refractive index contrast. Also, as in the previous images, the contrast reverses when going from 488 to 514 nm illumination.

aryl-(4-diethylphosphonate)-10-decylphosphonic acid ether SAM[16] deposited on a silicon wafer. Figure 7 shows the topography (Figure 7a) and NSOM images (Figures 7c,d) taken with $\lambda = 488$ nm and $\lambda = 514$ nm, respectively. Figure 7b shows a line trace taken from the position indicated by the dashed line in Figure 7a. This line trace shows that, equivalent to the image in Figure 2d, the dark stripe in the topography image is a trough ~20 nm (see Figure 7b) deep. From the measured depth, we can conclude that the film is either completely absent from this section or is perhaps a single monolayer thick. For either case we expect the film, if present at all in the trough, to be so thin that the optical properties of the material at the bottom of the trough can be approximated as being equivalent to that of the silicon. Surface aggregates with dimensions ranging from 50 to 800 nm in diameter and 30 to 70 nm tall are also present throughout the topography image. Since the topography image (Figure 7a) and the NSOM images (Figures 7c,d) have the same features, the source of contrast (topography induced, or true optical) cannot be determined by inspection.

Our goal is to understand the contrast in the NSOM images of Figure 7 quantitatively. Since the silicon substrate has a high reflectivity compared to the reflectivity expected for the film, it is possible that the contrast is due only to changes in the tip−silicon gap caused by the presence of the film. An analysis of the retract curve obtained over the silicon substrate will allow us to determine whether or not this is the case. Figure 8a shows the NSOM retract curve acquired with the tip positioned over the trough at the location indicated by the X in the topography image (Figure 7a) prior to acquiring the image of Figure 7d. In Figure 8b, an enlarged view of the same curve (Figure 8a) is

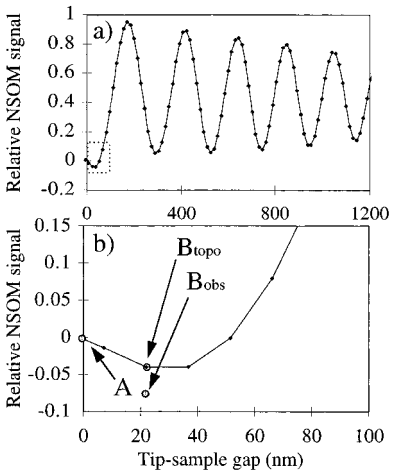

Figure 8. NSOM retract curve obtained with the NSOM tip positioned over the trough indicated by the X in Figure 7a. An enlarged version of the portion indicated by the dashed box in Figure 8a is shown in Figure 8b. *A* is the signal observed when the tip is over the trough. B_{topo} is the signal expected if the contrast is due only to a change in the tip−silicon distance, and B_{obs} is the observed signal over the film. This difference in the two signals (approximately one factor of 2 B_{obs}) is due to the optical properties of the film.

shown. When the tip is positioned at point B (see Figure 7d), it is 35 nm from the silicon surface (but only ~15 nm from the film as required by the feedback circuit). If the contrast observed in the image of Figure 7c is due only to the change in tip−silicon distance, then the signal can be read directly from the retract curve of Figure 8 at a distance of 20 nm. This signal,

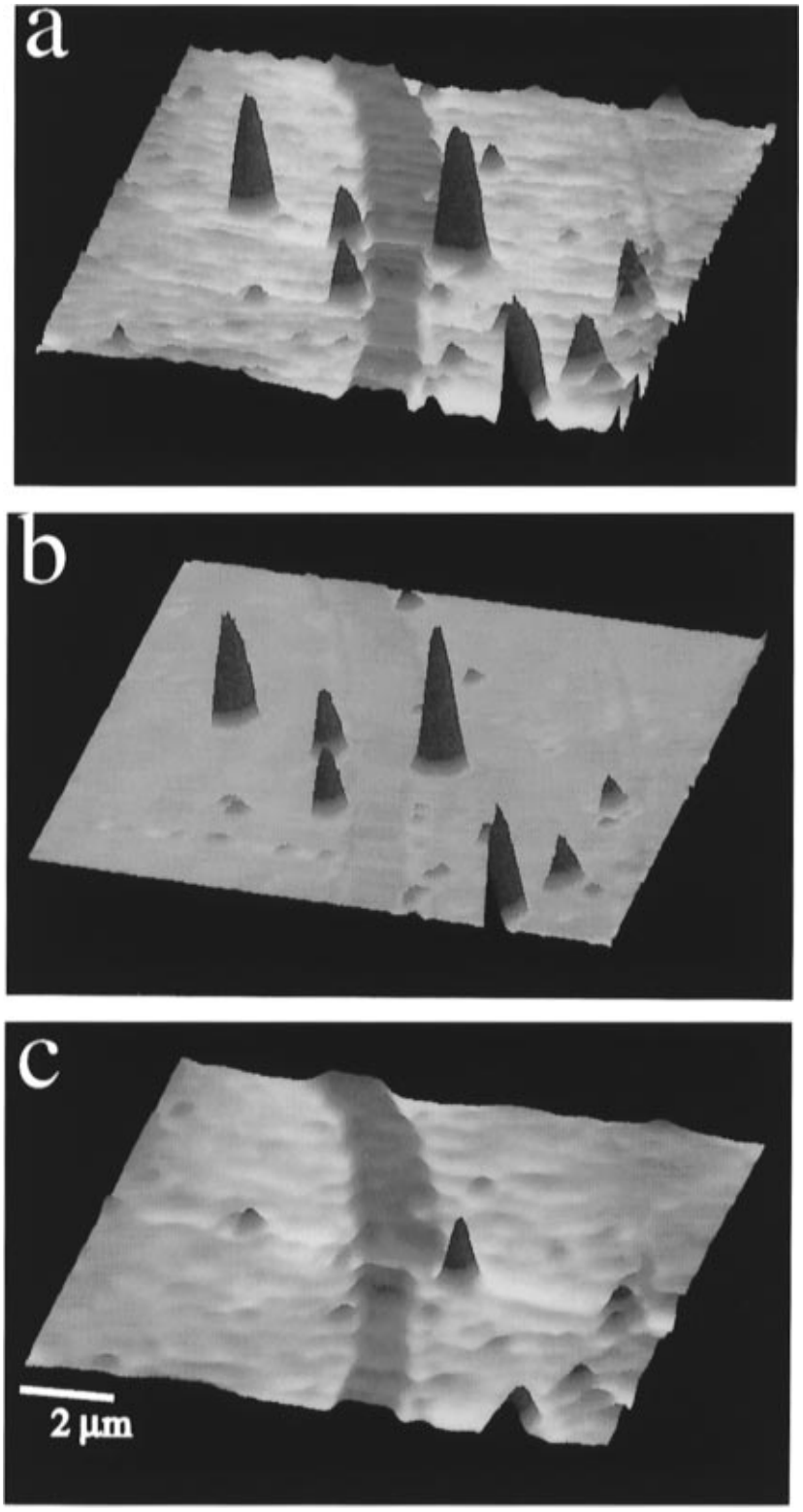

Figure 9. Separating true optical contrast from z-contrast. Part a is the same image as Figure 7d displayed as a surface plot. The topography image in Figure 7a and the retract curve obtained for $\lambda = 514$ nm (Figure 8) were used to simulate the image of part b, also displayed as a surface plot. This image represents the contribution of z-contrast in the image of part a. The image of part c results from subtracting the image of part b from the image of part a. The contrast remaining in the image of part c is due only to changes in the refractive index of the sample. Note that the signal observed over the trough is relatively unchanged, but the signal over the clusters is strongly attenuated and is approximately equal to the signal observed for the rest of the multilayer film.

denoted B_{topo} in Figure 8b, is not equal to the observed signal (B_{obs}). The difference between B_{topo} and B_{obs} (about a factor of 2) is attributed to the optical properties of the film.

An important consequence of the above analysis is that the retract curve of Figure 8 provides a means for determining the contribution of z-contrast to the total contrast observed in the dual mode NSOM image of this sample (reproduced as a surface plot in Figure 9a). By using the topography image of Figure 7a and the retract curve of Figure 8, it is possible to simulate a z-contrast image for this sample. Figure 9b shows the result of this simulation. Just as is demonstrated for a single point B, this simulation fails to quantitatively predict the actual contrast

in the image as can be seen by comparing the images of Figures 9a,b. Since the image of Figure 9b represents the contribution of z-contrast to the total contrast of Figure 9a, subtracting the image of Figure 9b from the image of Figure 9a produces an image representing the true optical (i.e., refractive index) contrast of the sample. The result of this subtraction is shown in Figure 9c. The immediate conclusions made from this image are (1) the material of the trough has a different refractive index than the multilayer material, as expected, and (2) the flattening of the signal at the locations of the aggregates indicates that the aggregates have the same refractive index as that of the multilayer film and are most likely the same material as that of the rest of the film. These conclusions could not have been made without removal of the topography induced contrast. The ability to remove this unwanted contrast represents the most important advantage of the dual mode technique over conventional illumination mode NSOM.

Conclusion

A dual mode NSOM configuration has been demonstrated as a powerful technique for characterizing organic thin films on opaque substrates. The contrast in dual mode NSOM images depends strongly on the interference effects between the incident and reflected modes as observed by the oscillations in the retract curve. By acquiring both a dual mode NSOM image and the retract curve, it is possible to simulate a z-contrast image from the retract curve and the topography image. Quantitative separation of the true optical contrast from the z-contrast is achieved by subtracting a simulated image of z-contrast from the original NSOM image. This separation allows for improved image interpretation and makes reflection NSOM a more viable alternative for high-resolution optical microscopy.

Acknowledgment. The authors acknowledge Professor Catherine J. Page and Grace Ann Neff of the University of Oregon Chemistry Department for supplying the SAM sample, Dr. Rod Sterling of NRC Canada for supplying the aluminum/glass sample, and Digital Instruments for supplying the grating sample. We also acknowledge Jessie DeAro, Grace Credo, and Professor David Awshalom and his group in the UCSB Physics Department for many useful discussions. This work was supported by NSF Grant CHE-9501773 and the Camille and Henry Dreyfus Foundation.

References and Notes

(1) Betzig, E.; Trautman, J. K.; Harris, T. D.; Weiner, J. S.; Kostelak, K. L. *Science* **1991,** *251*, 1468.
(2) Betzig, E.; Trautman, J. K. *Science* **1992**, *257*, 189.
(3) Blatchford, J. W.; Gustafson, T. L.; Epstein, A. J.; Vanden Bout, D. A.; Kerimo, J.; Higgins, D. A.; Barbara, P. F.; Fu, D.-K.; Swager, T. M.; MacDiarmid, A. G. *Phys. Rev. B* **1996**, *54*, R3683.
(4) Buratto, S. K. *Curr. Opin. Solid State Mater. Sci.* **1996**, *1*, 485.
(5) Higgins, D. A.; Barbara, P. F. *J. Phys. Chem.* **1995**, *99*, 3.
(6) Higgins, D. A.; Reid, P. J.; Barbara, P. F. *J. Phys. Chem.* **1996**, *100*, 1174.
(7) Hwang, J.; Tamm, L. K.; Böhm, C.; Ramalingam, T. S.; Betzig, E.; Edidin, M. *Science* **1995**, *270*, 610.
(8) Grober, R. D.; Harris, T. D.; Trautman, J. K.; Betzig, E.; Wegscheider, W.; Pfeiffer, L.; West, K. *Appl. Phys. Lett.* **1994**, *64*, 1421.
(9) Hess, H. F.; Betzig, E.; Harris, T. D.; Pfeiffer, L. N.; West, K. *Science* **1994**, *264*, 1740.
(10) Levy, J.; Nikitin, V.; Kikkawa, J. M.; Cohen, A.; Samarth, N.; Garcia, R.; Awschalom, D. D. *Phys. Rev. Lett.* **1996**, *76*, 1948.
(11) Trautman, J. K.; Betzig, E.; Weiner, J. S.; DiGiovanni, D. J.; Harris, T. D.; Hellman, F.; Gyorgy, E. M. *J. Appl. Phys.* **1992**, *71*, 4659.
(12) Valaskovic, G. A.; Holton, M.; Morrison, G. H.; *J. Microscopy (Oxford)* **1995**, *179*, 29.
(13) Weston, K. D.; DeAro, J. A.; Buratto, S. K. *Rev. Sci. Instrum.* **1996**, *67*, 2924.
(14) Cline, J. A.; Isaacson, M. *Appl. Opt.* **1995**, *34*, 4869.
(15) Lee, H.; Kepley, L. J.; Hong, H.-G.; Mallouk, T. E. *J. Am. Chem. Soc.* **1988**, *110*, 618.
(16) Neff, G. A.; Page, C. J.; Meintjes, E.; Tsuda, T.; Pilgrim, W.-C.; Roberts, N.; Warren, W. W., Jr. *Langmuir* **1996**, *12*, 238.
(17) Prof. C. Page. Private communication.
(18) Betzig, E.; Finn, P. L.; Weiner, J. S. *Appl. Phys. Lett.* **1992**, *60*, 2484.
(19) Toledo-Crow, R.; Yang, P. C.; Chen, Y.; Vaez-Iravani, M. *Appl. Phys. Lett.* **1992**, *60*, 2957.
(20) Betzig, E.; Grubb, S. G.; Chichester, R. J.; DiGiovanni, D. J.; Weiner, J. S. *Appl. Phys. Lett.* **1993**, *63*, 3550.
(21) From electroluminescence NSOM experiments, for example, see: Buratto, S. K.; Hsu, J.W. P.; Trautman, J. K.; Betzig, E.; Bylsma, R. B.; Bahr, C. C.; Cardillo, M. J. *J. Appl. Phys.* **1994**, *76*, 7720. Where the tip is used as a detector, an rough estimate of the collection efficiency was determined to be an order of magnitude larger than the transmission efficiency measured with far-field optics.
(22) Cline, J. A.; Barshatzky, H.; Isaacson, M. *Ultramicroscopy* **1991**, *38*, 299.
(23) Fischer, U. Ch.; Dürig, U. T.; Pohl, D. W. *Appl. Phys. Lett.* **1988**, 52, 249.
(24) Courjon, D.; Vigoureux, J. M.; Spajer, M.; Sarayeddine, K.; Leblanc, S. *Appl. Opt.* **1990**, *29*, 3734.
(25) Born, M.; Wolf, E. *Principles of Optics*, 4th Ed.; Pergamon Press: Oxford, 1970; p 279.
(26) Vigoureux, J. M.; Girard, C.; Courjon, D. *Opt. Lett.* **1989**, *14*, 1039.
(27) Novotny, L.; Pohl, D. W.; Regli, P. *J. Opt. Soc. Am. A* **1994**, *11*, 1768.
(28) Grober, R. D.; Rutherford, T.; Harris, T. D. *Appl. Opt.* **1996**, *35*, 3488.